Chapter – 5

Structural modulation, oriented intergrowth of rocksalt and spinel in equimolar multicomponent {Co(Cr/Mg)FeMnNi}-oxide and its derivatives

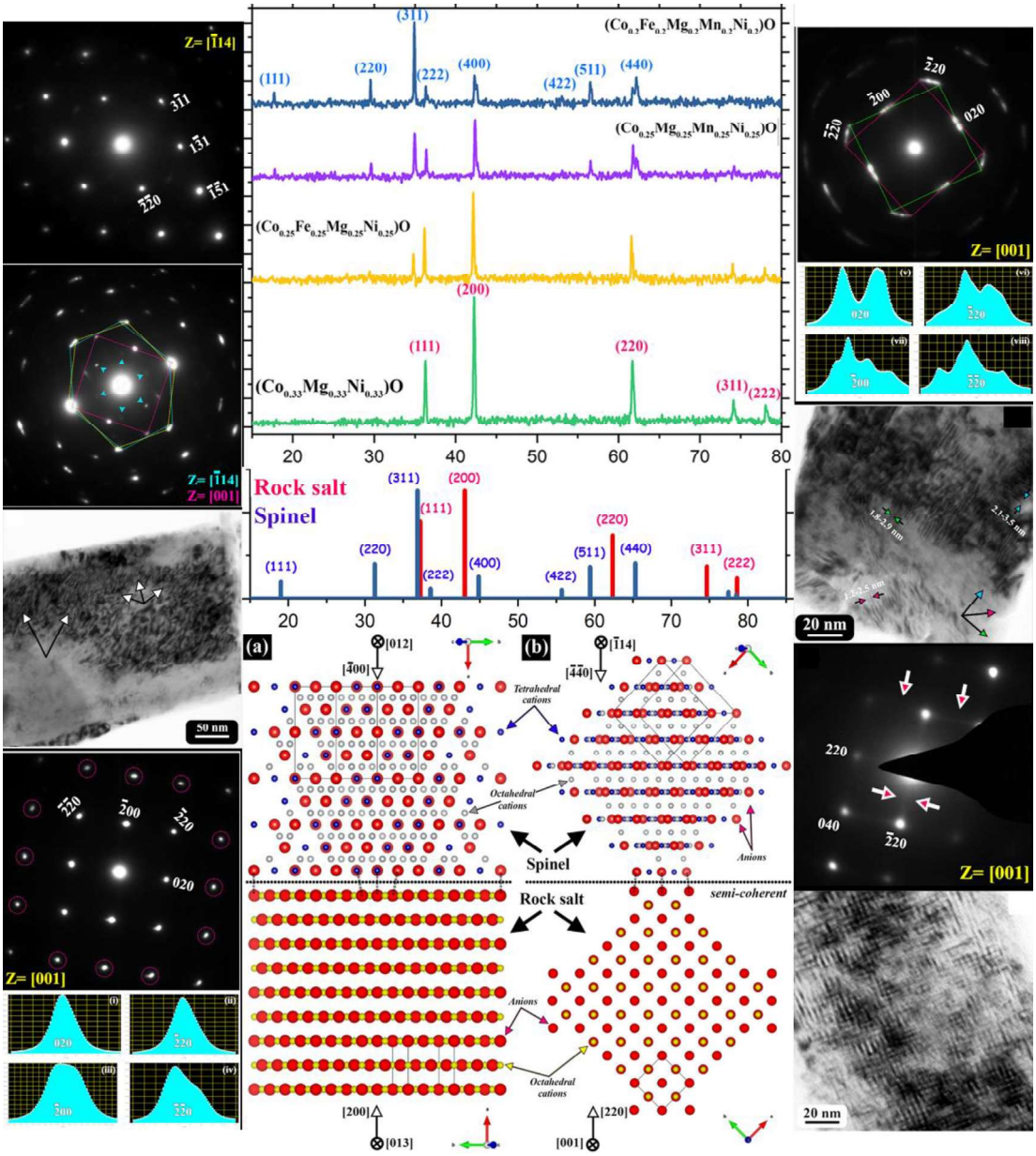

5.1. Introduction

Spinel and rocksalt forming high entropy oxides (HEOs)/ multicomponent oxides (MCOs) have garnered tremendous attention in the recent past owing to their favourable properties making it frontrunner candidates for their use in the field of energy conversion, storage and catalysis [1-7]. Right after the discovery of rocksalt HEO in (CoCuMgNiZn)O, less than a decade ago [8], successful synthesis of phase-pure spinel forming HEO in $(CoCrFeMnNi)_3O_4$ was reported a few years later [9], and subsequently a plethora of other HEO forming compositions were reported from each family of ceramic crystal structure [10,11]. A lot of groups have investigated these two special compositions since then, with primary focus on their functional properties [12-15]. Several substitutions to explore the composition-phase space have also been reported [16,17]. However, phase stability, microstructural evolution and the mechanism behind synergistic effect of entropic stabilization in these HEOs has been comparatively less explored [18-20]. There are couple of major schools of thought regarding the phase formation and stability of such multicomponent metallic oxides. The overwhelming belief that stabilization of a homogeneous disordered single-phase solid-solution stems from the dominance of configurational entropy of mixing in HEOs, sits on one hand [21, 22]. On the other hand, enthalpic penalties induced precipitation of related multicomponent secondary phases and/or defect microstructure formation has also been explored by a few research groups [23,24]. However, direct experimental evidences for such deviations are scarce. Additionally, the spinel crystal structure is relatively more complex than rocksalt counterpart owing to the degrees of freedom of void filling by cations, rendering it amenable to ordering, phase separation or distortions [25-30].

The current work has been carried out to understand the stability and phase-pure nature of the original spinel forming HEO. In order to arrive at satisfactory conclusions from

previously unreported experimental evidences, it is necessary to accumulate findings from its derivative lower-order oxides. It has been found out that equimolar ternary (CoMgNi)-oxide with rocksalt structure gives rise to phase-pure spinel structure upon partial substitution by Mn- and Fe-ions. This gives rise to $(CoFeMgMnNi)_3O_4$ single-phase spinel forming MCO, which is being reported for the first time. However, structural modulation and oriented inter-growth of related phases sharing coherent/semi-coherent boundaries in both the ternary and quinary MCO and HEO respectively can be discerned, which was previously not envisaged. Furthermore, phase separation event along specific crystallographic directions, although at its nascent stage, is found to influence the microstructural formation in the first ever reported $(CoCrFeMnNi)_3O_4$ spinel HEO.

5.2. Materials and methods

Multicomponent, equimolar oxides of (CoFeMgMnNi), (CoCrFeMnNi) and its binary, ternary and quaternary derivatives i. e. (MgNi)-oxide, (CoNi)-oxide, (CoMgNi)-oxide, (CoFeMgNi)-oxide and (CoMgMnNi)-oxide have been synthesized by solid-sate synthesis route due to the ease of materials handling and probability of success. Starting precursor oxides i. e. Co(II,III)O, Cr(III)O, Fe(II,III)O, MgO, Mn(III)O and NiO (>99.8 at% purity) were procured from either Alfa Aesar or Sigma Aldrich. The oxides in powder form were mixed in stoichiometric proportions for all the binary, ternary, quaternary and quinary compositions before they were mixed thoroughly in a mortar and pestle. Mixed equimolar ternary oxide of (CoMgNi) was further ball milled for 40 h in a Retsch PM400 planetary ball mill in dry environment using zirconia vial and balls at 200 rpm with 10:1 ball to powder ratio. During ball milling, the milling process was paused for 30s after every 60s of milling to avoid dynamic recrystallization. In order to study the phase evolution in the mixed powder, samples were collected after 5h, 15h and 40h of milling. The collected samples were characterized by X-ray diffraction (XRD) in a Rigaku MiniFlex600 table top

X-ray diffractometer with Cu-K_α (λ= 1.54 Å) radiation operated at 40 kV accelerating voltage with 15 mA tube current.

Precursor oxides, mixed in stoichiometric proportions, for all the binary, ternary, quaternary and quinary compositions were compacted in a uniaxial hydraulic press with 4T load to produce the green compacted pellets of ~12 mm diameter with ~4-5 mm thickness. The green compacted pellets were sintered at ~1473 K for 10 h in air before they were water quenched. Quinary (CoFeMgMnNi)-oxide was also sintered at 1473 K for 100 h, in addition to the 10 h sintering and it was then water quenched. Additionally, the ternary (CoMgNi)-oxide was aged at 723 K for 120 h in air and the it was water quenched. Sintering and ageing treatments were carried out in a platinum crucible with the lid on. In order to maintain perfect stoichiometry and avoid contamination, a number of pellets with identical composition were stacked together in the platinum crucible and the pellet from the centre of the stack was taken for further studies. Sintered, quenched and aged multicomponent oxides were characterized by XRD using a Malvern Panalytical high-resolution X-ray diffractometer with Cu-K_α (λ= 1.54 Å) and Co-K_α (λ= 1.79 Å) radiations. The diffractometer was operated 40 kV accelerating voltage with 40 mA tube current. The as-synthesized and aged multicomponent oxides were studied in a Tecnai G2 T20 transmission electron microscope (TEM). For TEM observation, thin slices were obtained from sintered, quenched and aged pellets by cutting the pellets with a low-speed saw. A slice from the center of the pellet was crushed to powder. The crushed powder was suspended in ethanol and was ultrasonicated for 15 minutes before it was drop-cast onto a carbon coated copper grid of ~3mm diameter. The XRD patterns were simulated by indigenously developed code and the structural models were developed by Vesta^{TM} software.

5.3. Results

In the XRD pattern of the as mixed equimolar mixture of Co(II,III)O, MgO and NiO (Figure 5.1a), individual diffraction peaks of the precursor oxide phases could be easily discerned. The Co(II,III)O exists both in spinel and rocksalt structures as evident from the XRD peaks marked by blue solid triangles and hollow open circles in red. MgO and NiO exist exclusively in rocksalt structure as marked by red close circles and black filled close circles respectively. The diffraction peaks of MgO and NiO are almost overlapping, which may be justified by the nearly similar lattice parameter and structure of the two oxides. The diffraction peaks of CoO with rocksalt structure appears very close to the MgO and NiO diffraction peaks due to its similar structure, however with a slightly larger lattice parameter. The experimentally observed diffraction patterns (Figure 5.1a) show excellent match with the simulated diffraction patterns (Figure 5.1b) of rocksalt and spinel structures with $a_{spinel} \sim 8.1$ Å *and* $a_{rocksalt} \sim 4.2$ Å. The lattice parameters of MgO, NiO and CoO are *a~4.21 Å, a~4.15 Å and a~4.26 Å* respectively. However, the lattice parameter of Co_3O_4 with spinel structure is *a~8.08 Å*, which is almost double (lattice parameter ratio~ 1.89) of the lattice parameter of the rocksalt phase. The structural relationship between the rocksalt phase and the spinel phase will be discussed in terms of their nature of void filling and ionic radii in the discussion section of the communication.

After 5h of milling, the XRD peaks (Figure 5.1a) becomes broad due to the refinement of particle size and accumulation of strain in the lattice of the crystals. The peaks corresponding to the spinel phase continue to exist. There is a sharp reduction in the intensity of the peaks corresponding to the rocksalt phase and the peaks corresponding to the CoO rocksalt phase cannot be distinctly observed. It appears as a shoulder to the peaks corresponding to the NiO and MgO rocksalt phases. It may be inferred that solid solutioning starts at the initial stages of milling. NiO and MgO acts as the host lattice in which CoO

with rocksalt structure starts getting incorporated. After 15h of milling, the peaks (Figure 5.1a) are further broadened with reduction of intensity as strain continues to get accumulated with simultaneous reduction in the particle size. The peaks corresponding to the CoO phase with rocksalt structure are completely merged with the peaks of the NiO and MgO phases. After 40h of milling, only the spinel phase is observed distinctly and the rocksalt phase is observed as a shoulder to the spinel phase.

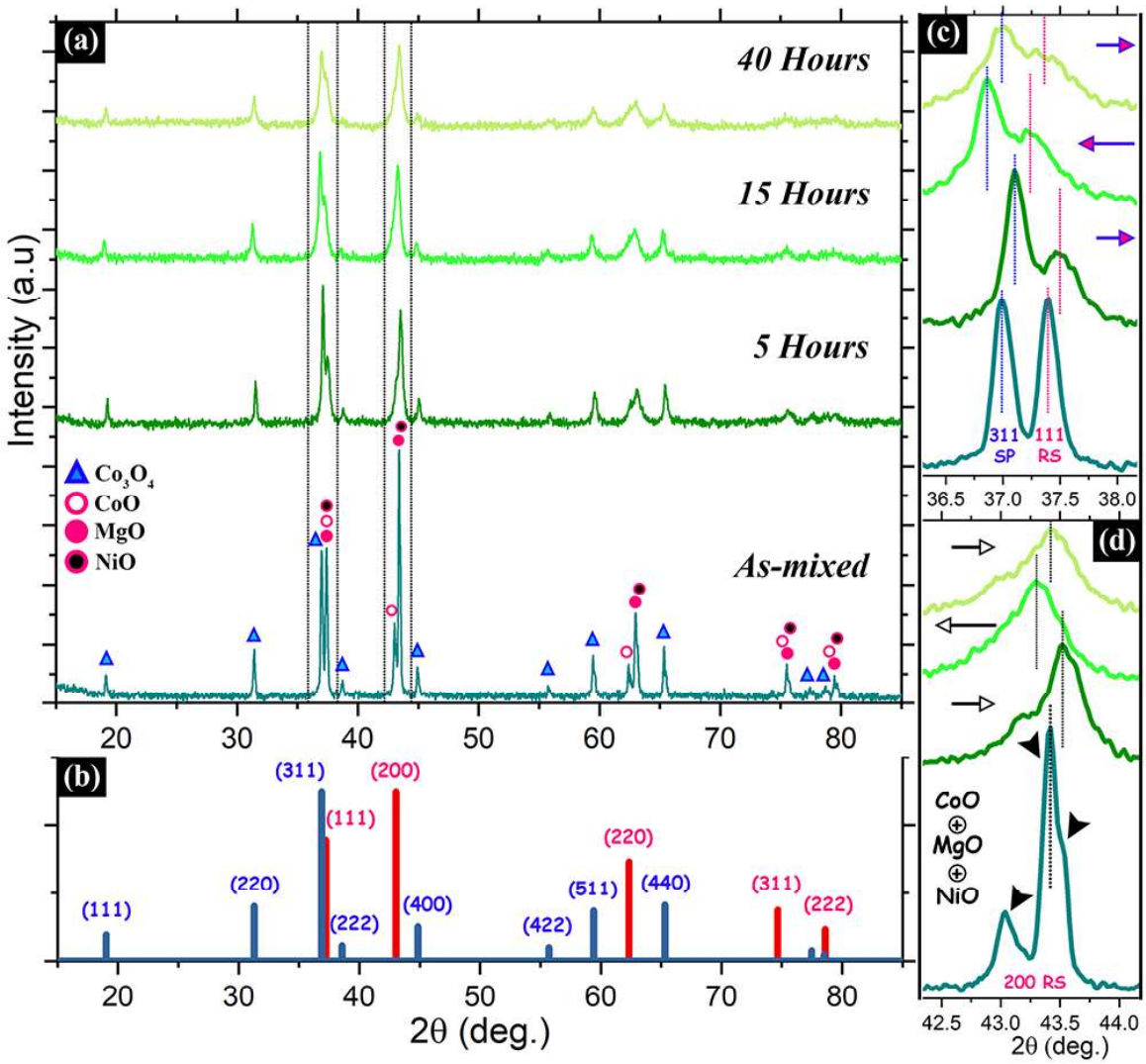

Figure 5.1: (a) X-ray diffraction (XRD) patterns of equimolar (CoMgNi)-oxide powder in the as-mixed condition and after 5h, 15h, 40h of ball milling. (b) Simulated XRD pattern of cubic rocksalt (a ~ 4.2 Å) in red and cubic spinel (a ~ 8.1 Å) in blue respectively. (c) Magnified view of 311 peak of cubic spinel and 111 peak of cubic rocksalt in as-mixed condition and after 5h, 15h and 40h of ball milling (d) Magnified view of the evolution of 200 peak of cubic rocksalt phase in the as-mixed condition and after 5h, 15h and 40h of ball milling.

It may be inferred that after 40h of milling solid solution phase consisting of spinel and rocksalt is formed in the initial stoichiometric mix of the elemental oxide powder. A magnified view of the evolution of the 311 peak of the spinel phase and the 111 peak of the rocksalt phase with the progress of milling is given in Figure 5.1c. As stated earlier, with the progress of milling both the peaks are broadened and they start to merge with one another. However, there is a slight rightward shift of the peaks after 5h of milling, which becomes a net leftward shift after 15h of milling and again a slight rightward shift after 40h of milling. Change in d-spacing due to progressive solid solutioning is expected to be uni-directional in nature. In this case, switching of the shift direction may be attributed to the change in d-spacings and cell volume due to the accumulation of strain and vacancies in the lattice of the spinel and rocksalt based solid solution phases and the attempt of the phase mixture to optimize its vacancy concentration, composition etc. Likewise, the magnified view of the 200 peak of the rocksalt-based CoO, MgO and NiO phases (Figure 5.1d) shows initiation of peak merger after 5h of milling. After 15h of milling, individual peaks of CoO, MgO and NiO phases are not observed indicating that the process of solid solution phase formation is mostly complete after 15h of milling. However, along with the peak broadening, a slight rightward shift after 5h of milling, a net leftward shift after 15h of milling and a slight rightward shift after 40h of milling is observed. This may also be attributed to the accumulation of strain, increase in vacancy concentration in the rocksalt based solid solution phase and the attempt of the phase to optimize its strain, vacancy concentration and composition. It will be substantiated further in the discussion section in terms of ionic radii of the species and the structural similarity between rocksalt and spinel phases.

XRD patterns of equimolar binary (MgNi)-oxide (in red), (CoNi)-oxide (in blue) and ternary (CoMgNi)-oxide (in green) powder after sintering at 1473 K for 10 h are given in

Figure 5.2. In the binary (MgNi)-oxide exclusively rocksalt phase with *a~4.21 Å* lattice parameter is observed. In the binary (CoNi)-oxide cubic rocksalt phase with *a~4.20 Å* and a cubic spinel phase with *a~8.25 Å* lattice parameters are observed. In the ternary (CoMgNi)-oxide only cubic rocksalt phase with *a~4.20 Å* lattice parameter is observed. In the diffraction pattern of this ternary oxide a small undulation corresponding to the 220 peak of a spinel phase is observed. However, the undulation is so small, it may not be used as a confirmation for the existence of the spinel phase.

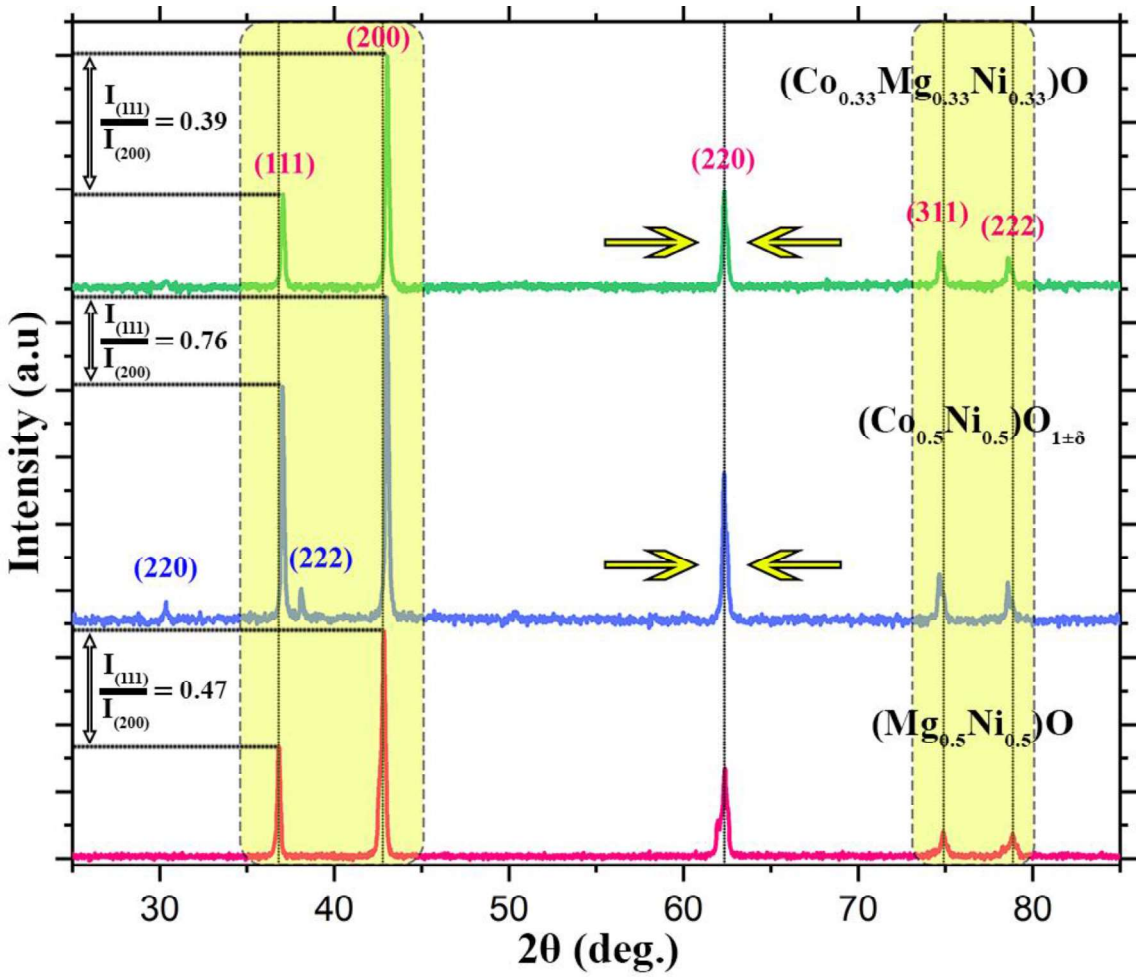

Figure 5.2: X-ray diffraction (XRD) patterns of equimolar binary (MgNi)-oxide, (CoNi)-oxide and ternary (CoMgNi)-oxide powder after sintering at 1473 K for 10h followed by water quenching. In all three compositions cubic rocksalt phase forms as the major phase, however, with varying intensity ratios of 111 and 200 diffraction peaks.

In order to further investigate the existence of the spinel phase, XRD patterns of the (CoMgNi)-oxide after sintering at 1473 K for 10h in the pellet and powder form has been compared (Figure 5.3a). In the XRD pattern of the pellet, a distinct 220 peak for spinel has been observed and other spinel peaks overlap with the peaks of the rocksalt phase. It may be due to the low volume fraction of the spinel phase and its oriented growth with the rocksalt phase. It is noteworthy that the lattice parameter of the spinel phase is almost double of the rocksalt phase as stated earlier. The normalized intensity plot of the experimental XRD patterns of the pellet and the crushed powder as shown in Figure 5.3a are given in Figure 5.3b. It is confirmed that the Compton inelastic background of the powder after crushing the sintered and quenched pellet is higher than the sintered and quenched pellet itself. Due to the high Compton background in the XRD pattern of the crushed powder of the sintered and quenched pellet, the low intensity 220 peak of spinel may remain invisible. It is understandable that crushing of the pellet introduces strain that increases the Compton background scattering in the crushed powder. It may be inferred that low volume fraction of the spinel phase, its oriented growth with the rocksalt phase and concomitant increase in the Compton background scattering leads to the almost invisibility of the low intensity 220 peak of the spinel phase in the crushed powder. Similar changes in XRD patterns in entropy stabilized oxides (ESOs) depending on processing conditions has been reported before.

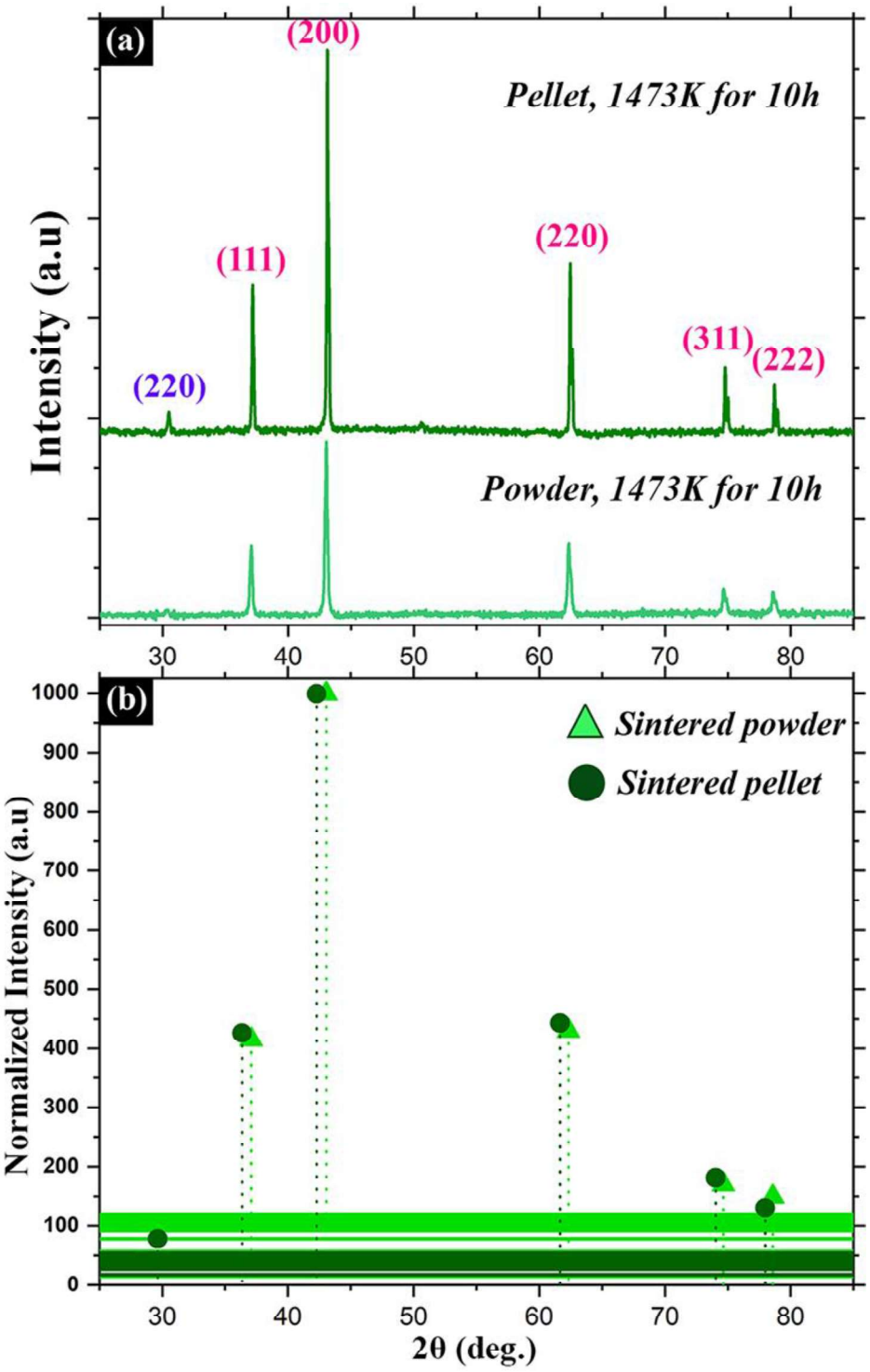

Figure 5.3: (a) X-ray diffraction (XRD) patterns of equimolar ternary (CoMgNi)-oxide powder (light green) and pellet (dark green) after sintering at 1473 K for 10h followed by water quenching. In the pellet, signature of cubic spinel phase is observed, which is absent in the powder. (b) Normalized intensity plots from the experimental XRD patterns of the powder (light green) and pellet (dark green). Compton modified scattering background is represented as bands with respective colours. Compton modified background for the powder being high, the low intensity spinel peak gets suppressed in the powder.

TEM bright field image (BF) and electron diffraction patterns of (CoMgNi)-oxide after sintering at 1473 K for 10h followed by water quenching are given in Figure 5.4(a-d). In the BF image (Figure 5.4c) mottled contrast indicating the presence of residual strain is observed. The corresponding diffraction patterns from z=[011] (Figure 4a), z=[125] (Figure 5.4b) and z=[013] (Figure 5.4d) may be indexed to a cubic rocksalt phase with *a~4.2 Å* lattice parameter. It is noteworthy that the diffraction patterns from a cubic spinel phase with double the lattice parameter will appear to be very similar from similar zone axes as will be demonstrated later in this communication. However, in case of a spinel phase some systematic extra spots should be observed, which are not present in the diffraction patterns. As the selected area diffraction patterns are obtained from very localized regions, the signature of cubic spinel phase is absent. This perfectly corroborates the XRD results, where it has been stated that the spinel phase is present in a very small volume fraction. Around the diffraction spots, diffuse scattering is observed (Figure 5.4a and 5.4d) and in some of the diffraction spots, geometric shape evolution and splitting is observed (Figure 5.4a and 5.4b). It will be discussed further in the subsequent sections. TEM DF image (Figure 5.4e) and its corresponding BF pair (Figure 5e inset) after ageing the sintered and quenched sample at 723K for 120h shows extensive fringe contrast along with the mottled contrast. Magnified version of the BF image in Figure 5.4e (inset) is given in Figure 5.4f. The fringe contrast is clearly visible in the image. The fringes are marked with arrows in the image. The spacing between consecutive fringe ranges from ~1.5-3.5 nm. In the diffraction pattern from the same region (Figure 5.5b) along z=[001], extensive splitting and arcing of spots with intensity modulation is observed. Different points in the diffracted arcs may be systematically joined together to bring out the symmetry shape corresponding to the four-fold [001] zone axis pattern of a cubic rocksalt phase with *a~4.2 Å* lattice parameter.

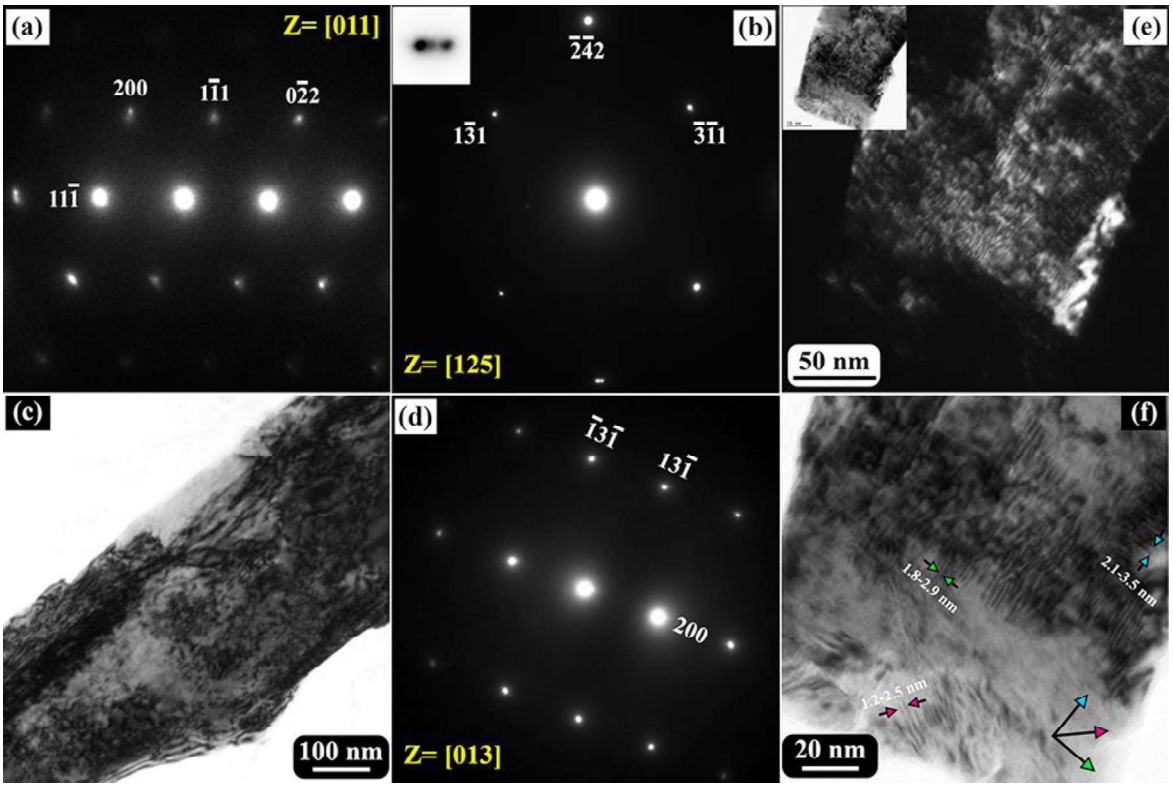

Figure 5.4: (a-d) Bright field image and selected area diffraction patterns along z=[011], z=[125] and z=[013] zone axes from ternary equimolar (CoMgNi)-oxide after sintering at 1473 K for 10 h followed by water quenching. The diffraction patterns may be indexed to a cubic rocksalt phase (a ~ 4.2 Å) with diffuseness and occasional spot splitting. Mottled contrast associated with strain fields is observed in the bright field image. (e) Centred dark field image and complementary bright field image (inset) from the same ternary equimolar (CoMgNi)-oxide after sintering at 1473 K for 10 h followed by ageing at 723 K for 120 h, in which parallel fringe with alternating contrast is observed. (f) Magnified bright field image of (e) showing multiply oriented fringes with ~1.5-3.5 nm spacing between them.

Two such symmetry shapes by joining the extreme ends of the arcs are shown in the figure with coloured dotted lines. It is observed that the symmetry shapes are rotated with respect to one another. Mutual rotation between two symmetry shapes formed by joining the extreme ends of the arcs is ~20°. It may be inferred that cubic rocksalt domains with mutual rotation among them do exist in the aged sample. It can be substantiated that the mutually rotated domains are developed during ageing by comparing a similar diffraction pattern along z=[001] from the sintered and quenched sample in Figure 5.5a. The diffraction pattern from the sintered and quenched sample (Figure 5.5a) along z=[001] may be indexed

to a cubic rocksalt phase with $a \sim 4.2$ Å lattice parameter. However, the arcing, splitting and modulation of intensity is absent in the lower order spots. Minor arcing and spot splitting are observed in the higher order spots (circled in the diffraction pattern in Figure 5.5a). This necessarily means that ternary, equimolar oxide tends to form a domain structure from the very beginning. However, there is a kinetics of such mutually rotated domain formation, due to the paucity of time this did not develop during sintering and quenching. It is further evidenced, when the intensity distribution of the lower order spots perpendicular to the individual g-vectors is plotted in one dimension. Intensity distribution plots are given below the corresponding diffraction patterns in Figure 5.5. The intensity distribution plots of the g-vectors for the sintered and quenched sample are mostly symmetric with a very minor skewness for the $\bar{2}\bar{2}0$ type spots. In comparison to that the intensity distribution plots of the diffraction spots for the sintered, quenched and aged sample shows multiple maxima with finite skewness. Formation of mutually rotated domains in sintered, quenched and aged sample manifests itself in the form of wavy fringe contrast in the BF and DF images as has been observed in Figure 5.4e and 5.4f. Formation of such mutually rotated domains leading to a fringe contrast and tweed morphology has been observed after long h of sintering and ageing in (CaCoFeMgNi)-oxide and (CoCuMgNiZn)-oxide respectively. It is understood that such tweed structures form in multicomponent oxide after long h of sintering and ageing in a bid to minimize its strain. It will be discussed further in the discussion section.

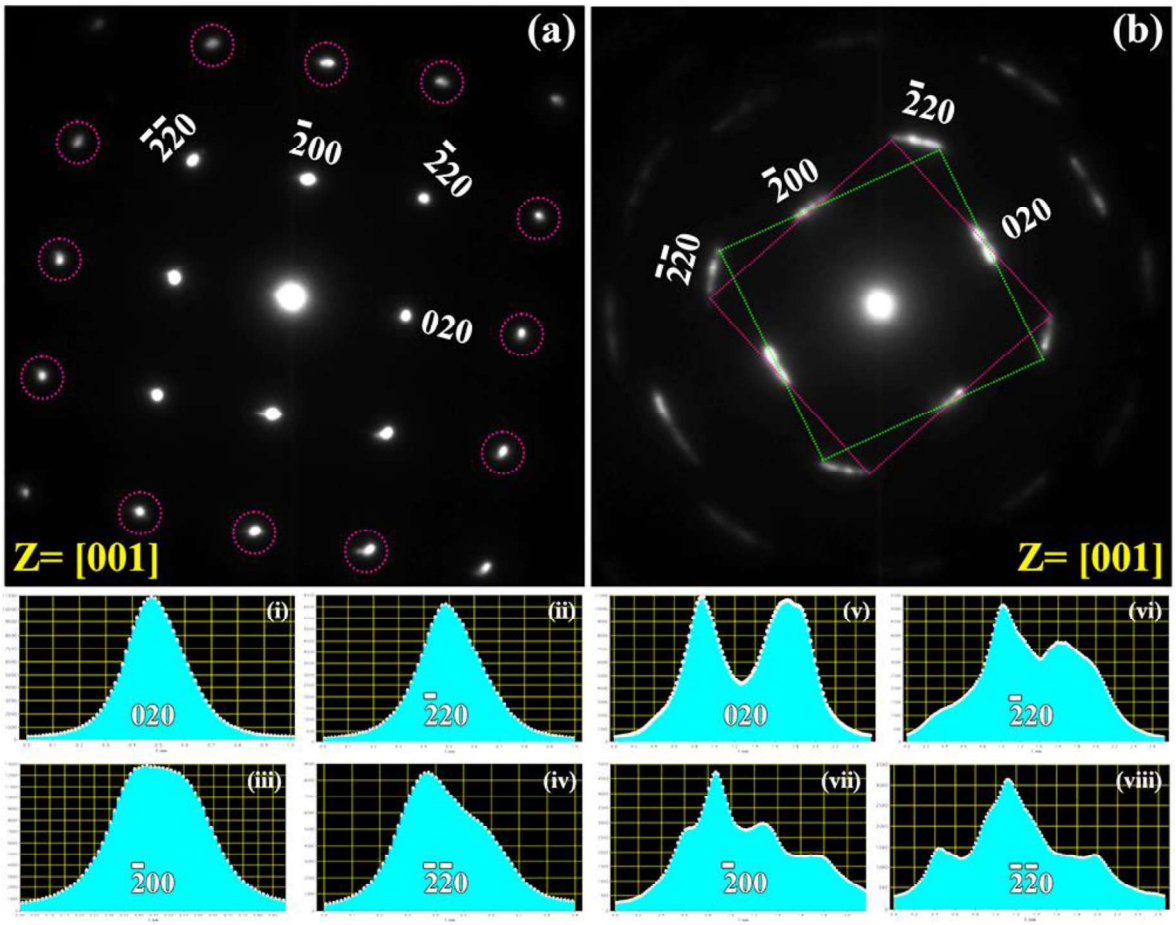

Figure 5.5: (a) Selected area electron diffraction pattern along z=[001] zone axis of (CoMgNi)-oxide after sintering at 1473 K for 10h followed by water quenching. Onset of splitting in the higher order spots (marked by dotted circles) is observed. (i-iv) Intensity distribution plots of 200 and 220 type spots are almost symmetrical. (b) Selected area electron diffraction pattern along z=[001] zone axis of (CoMgNi)-oxide after sintering at 1473 K for 10h, ageing at 723 K for 120h followed by water quenching. The diffraction spots are split and arced with modulation of intensity distribution. (v-viii) Intensity distribution plots of 200 and 220 type spots are not symmetrical with several maxima.

Ternary equimolar (CoMgNi)-oxide has been partially substituted with Fe-ion, Mn-ion and both Fe-, Mn-ion to form equimolar quaternary (CoFeMgNi)-oxide, (CoMgMnNi)-oxide and equimolar quinary (CoFeMgMnNi)-oxide. XRD patterns of the quaternary and quinary derivative oxides after sintering at 1473 K for 10h followed by water quenching is given in Figure 5.6. As reported earlier, (CoMgNi)-oxide after sintering and quenching forms cubic rocksalt phase with *a~4.2 Å* lattice parameter. Upon systematic addition of Fe-ions, in the quaternary (CoFeMgNi)-oxide after sintering at 1473 K for 10h followed by water

quenching the cubic rocksalt phase with *a~4.2 Å* lattice parameter continues to exist. However, the most intense 311 peak of a spinel phase with *a~8.4 Å* lattice parameter appears. Upon systematic addition of Mn-ions, coexistence of two-phase mixture of a cubic rocksalt with *a~4.2 Å* lattice parameter and a cubic spinel with *a~8.4 Å* lattice parameter is observed in the quaternary sintered and quenched (CoMgMnNi)-oxide. In the quinary (CoFeMgMnNi)-oxide, after sintering and quenching, predominantly a spinel phase with *a~8.38 Å* lattice parameter is observed. It is worth mentioning that the diffraction peaks of a cubic rocksalt phase with *a~4.2 Å* (half the lattice parameter of the cubic spinel phase) lattice parameter will overlap with the diffraction peaks of the spinel phase. It is further evidenced by the presence of shoulders in the 222, 400 and 440 diffraction peaks of the spinel phase. It should be noted that, to the best of the knowledge of the authors, quinary multicomponent (CoFeMgMnNi)-oxide has not been reported before. It has been investigated further by electron diffraction after sintering for different lengths of time, which will be reported in the subsequent sections.

TEM BF images and corresponding electron diffraction patterns from the same region of (CoFeMgMnNi)-oxide after sintering at 1473 K for 10h are given in Figure 5.7(a-d). In the BF images extensive mottled contrast is observed and the electron diffraction patterns along z=[001] and z=[$\bar{1}$14] may be indexed to a cubic spinel phase with *a~8.38 Å* lattice parameter. It is noteworthy that in the BF image in Figure 5.7d localized fringe contrast is observed. Magnified view of the fringe contrast is given in Figure 5.7d (inset). Existence of this linear Moire fringe contrast is indicative of two crystals with similar or nearly similar d-spacing are juxtaposed over one another with or without minor tilting [33]. As it has been stated earlier, the structure of spinel and rocksalt phase are quite similar. It may be the juxtaposition of a cubic rocksalt phase over a cubic spinel phase. However, due to the paucity of the diffraction evidence, it may not be confirmed at this stage.

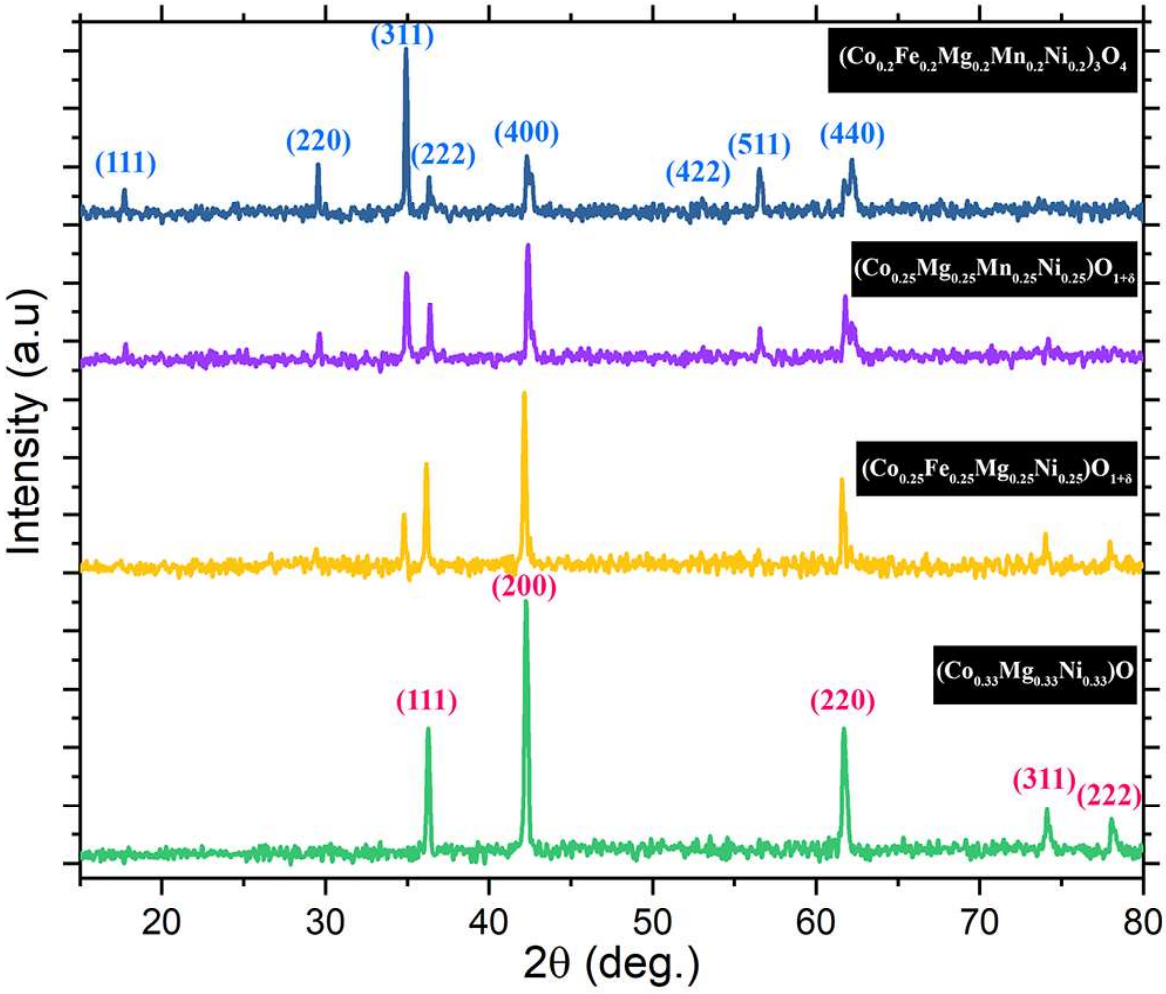

Figure 5.6: X-ray diffraction (XRD) patterns of (CoMgNi)-oxide with systematic addition of Fe- and Mn-ions after sintering at 1473 K for 10h followed by water quenching. With systematic addition of Fe- and Mn-ions the major phase in the equimolar multicomponent oxide changes from cubic rocksalt phase to cubic spinel phase.

TEM BF images from different regions, corresponding electron diffraction patterns and their inverted versions with the indexing for (CoFeMgMnNi)-oxide after sintering at 1473 K for 100 h followed by water quenching are given in Figure 5.8(a-f). In the BF image in Figure 5.8c, mottled and irregular fringe contrast is observed. Existence of such contrast may indicate presence of localized residual strain and structural modulation in the material. Corresponding electron diffraction pattern (Figure 5.8a), shows extensive spot splitting,

arcing and intensity modulation. The inverted version of the diffraction pattern is given in Figure 5.8b. The diffraction pattern may be indexed to a cubic spinel phase with *a~8.33 Å* lattice parameter and a cubic rocksalt phase with *a~ 4.15 Å* lattice parameter. The diffraction vectors for the cubic spinel phase and the cubic rocksalt phase along with their angular relationships and the ratios of the principal vectors are marked in Figure 5.8b in cyan and magenta colour respectively. The diffraction pattern may be indexed to a z=[$\bar{1}$14] zone axis pattern of a cubic spinel phase. It is noted that the first order reflections in this zone axis are weak (marked by cyan arrows in Figure 5.8a and dotted circles in Figure 5.8b) and the second order reflections are strong. The second order reflections are strong as they are common to both the spinel and the rocksalt phase. In addition, arcing, splitting and intensity modulation in the second order spots are observed. When the second order spots are systematically joined together with dotted lines (Figure 5.8a), it clearly brings out the two-fold symmetry shape corresponding to z=[$\bar{1}$14] zone axis of a cubic spinel phase, however, rotated with respect to one another. This clearly indicates that the spinel phase forms structurally modulated domains, which are rotated with respect to one another. Formation of such rotated domains has been reported for quinary (CaCoFeMgNi)-oxide and (CoCuMgNiZn)-oxide after long h of sintering or ageing. It will be discussed further in the discussion section. There are some additional diffraction spots in the diffraction pattern in Figure 5.8a and its inverted version in Figure 5.8b. Those spots are marked in magenta along with the ratio of the principal vectors. The spots are joined together with magenta dotted lines (Figure 5.8a), that brings out a four-fold symmetry shape. The additional spots may be indexed to a cubic rocksalt phase along z=[001] zone axis *a~ 4.15 Å* lattice parameter. It is due to the simultaneous presence of a cubic spinel phase with the rocksalt phase intensity modulation is observed in the diffraction pattern.

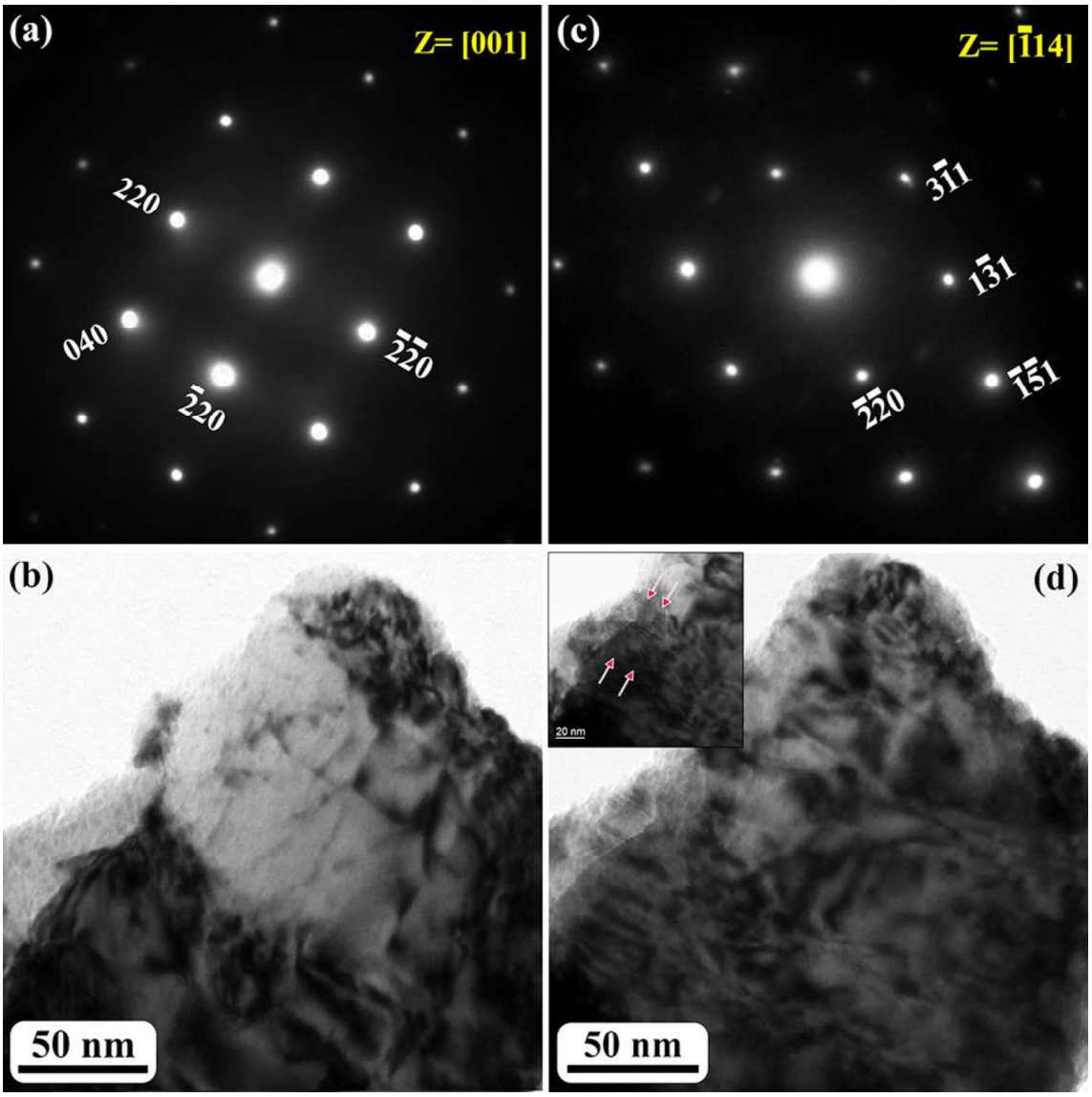

Figure 5.7: (a, c) Selected area electron diffraction patterns along z=[001] and z=[$\bar{1}$14] zone axes respectively and (b, d) bright field images of the multicomponent equimolar (CoFeMgMnNi)-oxide after sintering at 1473 K for 10h followed by water quenching. Electron diffraction patterns are indexed to a cubic spinel phase (a~8.38 Å). In the bright field images mottled contrast with occasional fringe contrast (Figure 7d inset) is observed.

It is noteworthy that there is an orientation relationship between the rocksalt phase and the spinel phase, which may be written as $[\bar{1}14]_{Spinel} \parallel [001]_{Rocksalt}$ and $(440)_{Spinel} \parallel (\bar{2}\bar{2}0)_{Rocksalt}$. BF image from a different region (Figure 5.8d) shows a domain like contrast in addition to the irregular fringe contrast. The corresponding electron diffraction pattern and its inverted version are given in Figure 5.8e and Figure 5.8f respectively. In this diffraction pattern also

modulation of intensity is observed and it may be indexed to z=[012] zone axis of a cubic spinel phase and z=[013] of a cubic rocksalt phase. The spots corresponding to the spinel phase, rocksalt phase, their principal vectors and their ratios are marked in cyan and magenta respectively. Similar orientation relationship is evident in this diffraction pattern. The orientation relationship is $[012]_{Spinel} \parallel [013]_{Rocksalt}$ and $(400)_{Spinel} \parallel (\bar{2}00)_{Rocksalt}$.

Effect of substitution of Cr-ions in place of Mg-ions in the quinary equimolar (CoFeMgMnNi)-oxide after sintering followed by quenching, which results into an equimolar quinary (CoCrFeMnNi)-oxide, has been studied by XRD and TEM. It is noteworthy that equimolar (CoCrFeMnNi)-oxide is the first ever reported single-phase spinel forming high entropy oxide (HEO). It is also the oxide form of the first reported high entropy Cantor alloy. In the XRD pattern of the sintered and quenched (CoFeMgMnNi)-oxide (Figure 5.9), cubic spinel phase with *a~8.38 Å* lattice parameter and cubic rocksalt phase with *a~4.2 Å* in minor proportion are observed. In the XRD pattern of the (CoCrFeMnNi)-oxide after sintering at 1473 K for 10h, cubic spinel phase with *a~8.36 Å* lattice parameter is predominantly observed. However, shoulders are observed in 222, 400 and 440 peaks, which can be directly indexed as the 111, 200 and 220 peak of a cubic rocksalt phase with half the lattice parameter. The XRD patterns of the same oxide after sintering and quenching, in pellet and powder form (Figure 5.9), have been compared and they do not show any significant difference except peak broadening and concomitant reduction in peak intensity. It may be inferred that in (CoCrFeMnNi)-oxide after sintering and quenching cubic spinel phase forms predominantly. However, there might be a possibility of oriented growth of cubic rock phase with half the lattice parameter within the spinel phase.

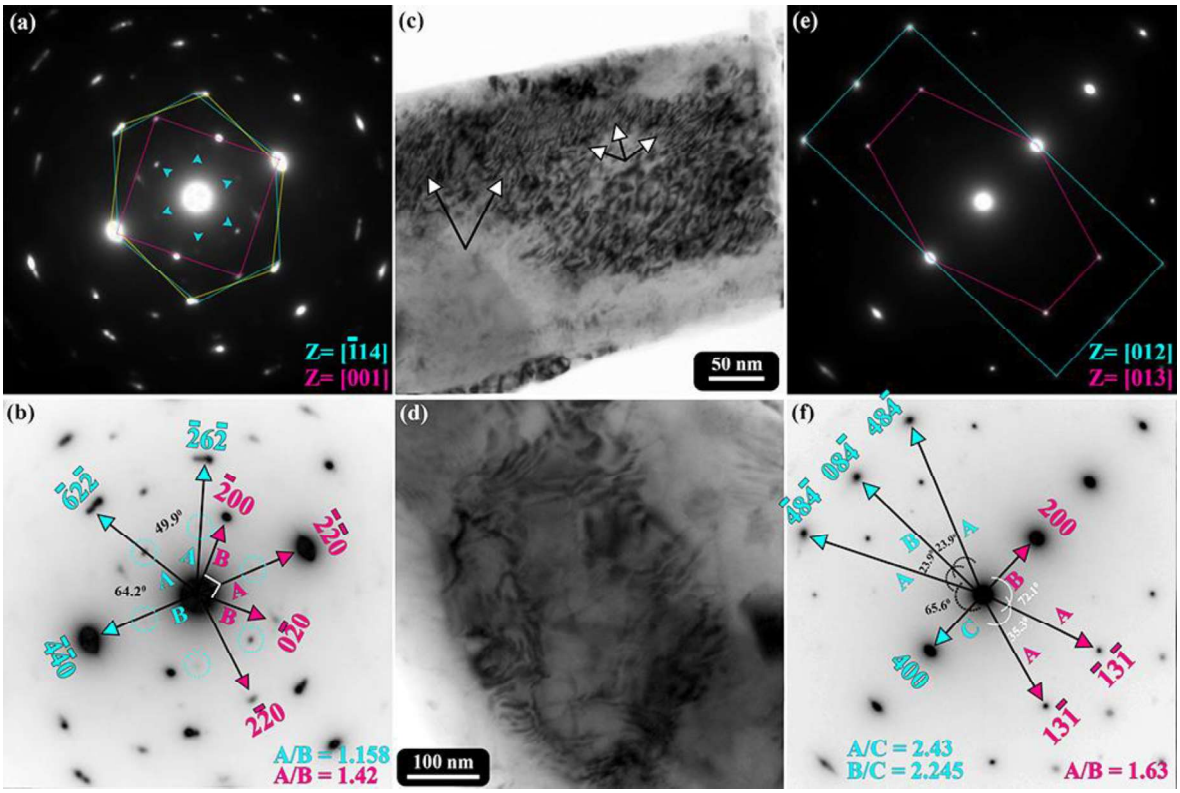

Figure 5.8: Selected area electron diffraction patterns and bright field images of (CoFeMgMnNi)-oxide after sintering at 1473 K for 100h followed by water quenching. The diffraction pattern in (a) is indexed to a cubic spinel phase, z=[$\bar{1}$14] zone axis along with a coexistent rocksalt phase, z=[001] zone axis. Indices of the diffraction spots, their angular relationships and ratios of principal vectors are given in (b), which is inverted with respect to (a). In the corresponding bright field image in (c), extensive fringe contrast (marked by arrows) within the mottled contrast is observed. The diffraction pattern in (e) is indexed to the same cubic spinel phase, z=[012] zone axis along with the coexistent cubic rocksalt phase, z=[013] zone axis. Indices of the diffraction spots, their angular relationships and the ratios of the principal vectors are given in (f), which is inverted with respect to (e). The corresponding bright field image in (d) shows domain like structure along with fringe contrast. Orientation relationship between the cubic spinel phase and the cubic rocksalt phase is evident.

TEM images and corresponding electron diffraction patterns of (CoCrFeMnNi)-oxide after sintering at 1473 K for 10h followed by quenching are given in Figure 5.10(a-f). In the electron diffraction pattern (Figure 5.10c) along z=[001], clear four-fold symmetry of the zone axis is observed. The diffraction pattern may be indexed to a cubic spinel phase with *a~8.36 Å* lattice parameter. It is noteworthy that the diffraction spots are diffused and a continuous streaking along 220 type vectors is observed.

It necessarily indicates the presence of continuous structural modulation in the multicomponent oxide. In the BF image (Figure 5.10a), a fine scale modulation is observed. In the magnified version of the BF image, given in Figure 5.10d, coexistence of structural modulation along two perpendicular directions is observed. The existence of such structural modulations leads to the formation of a domain morphology (marked in Figure 5.10d), which are ~5nm X 5nm is size. In the centred DF image (Figure 5.10b) with 220 spot under multibeam excitation, similar modulation is observed. The domains with alternate bright and dark contrast are marked in Figure 5.10b.

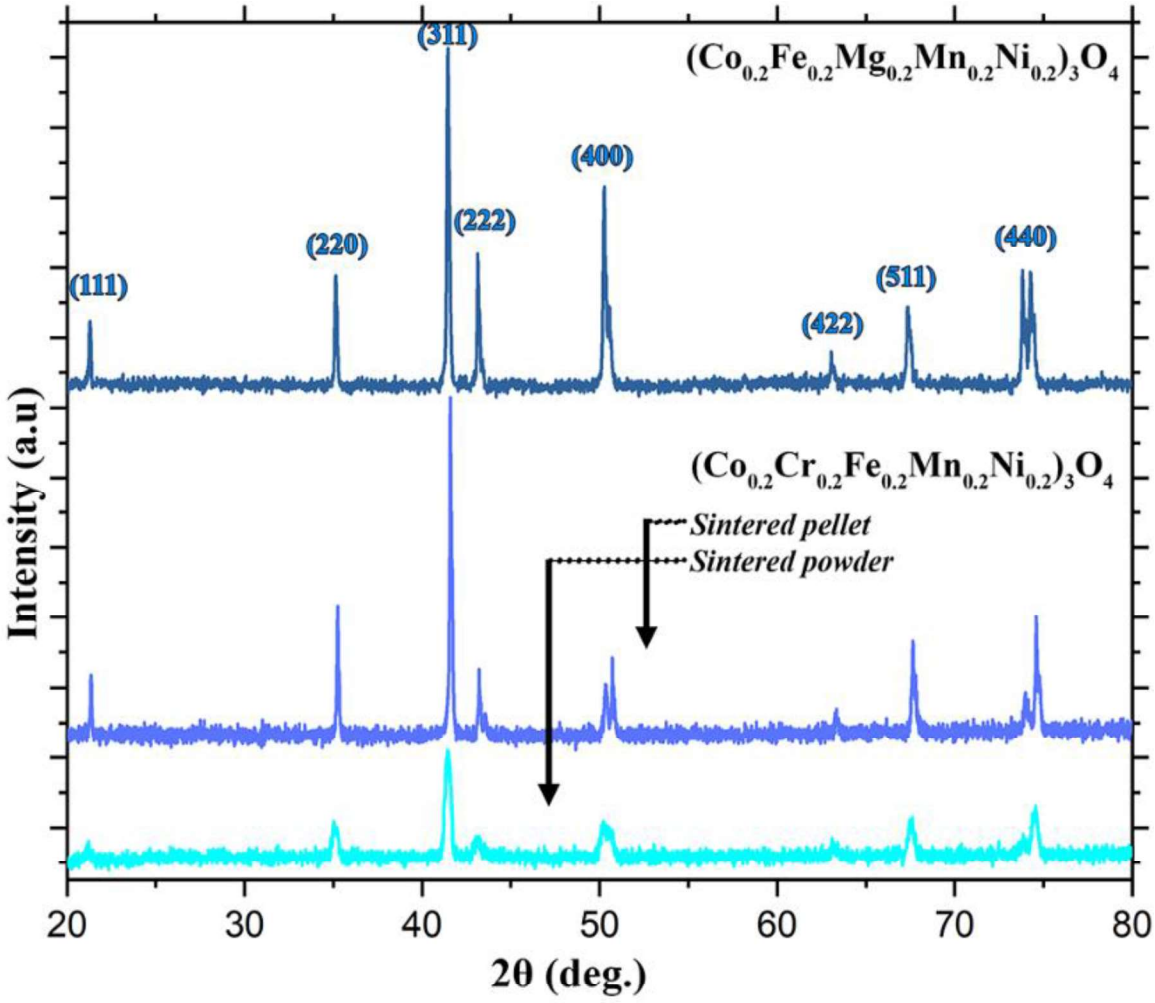

Figure 5.9: X-ray diffraction (XRD) patterns of (CoFeMgMnNi)-oxide and (CoCrFeMnNi)-oxide after sintering at 1473 K for 10h followed by water quenching. In both of the multicomponent oxides cubic spinel phase is observed to be the predominant phase with systematic peak splitting and shouldering.

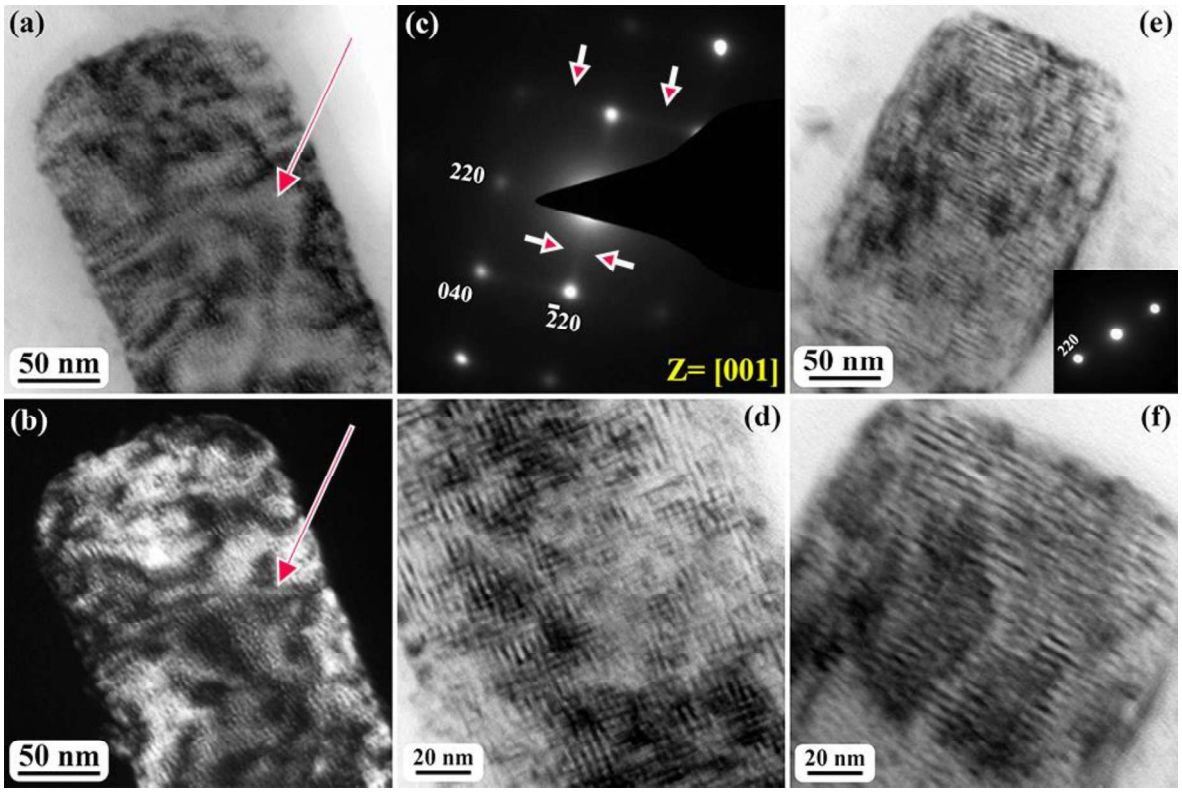

Figure 5.10: (a-f) Bright field, centred dark field and selected area electron diffraction patterns of (CoCrFeMnNi)-oxide after sintering at 1473 K for 10h followed by water quenching. The diffraction pattern in (c) is indexed to a cubic spinel phase, z=[001] zone axis. The diffraction spots are diffused with streaking along mutually perpendicular 220 type directions (marked with arrows). In the bright field image in (a) and corresponding centred dark field image in (b) modulation and formation of nanodomains are observed (marked with arrows). In two-beam bright field image in (e) and in (f) modulation along 220 direction is observed. Corresponding two beam diffraction pattern is given in the inset of (e). Cross penetration of modulation leading to the formation of domains is shown in the high magnification image in (d).

BF image of the same region with only 220 row of spots excited (Figure 5.10e) shows the modulation in only one direction perpendicular to the 220 reciprocal lattice vectors. The magnified version of the same region (Figure 5.10f) shows the modulation perpendicular to 220 type directions with modulation wavelength of ~5nm giving birth to a lamellar appearance. It may be inferred that the modulation develops in the spinel phase along 220 type directions. It will be discussed in detail in the discussion section.

5.4. Discussion

Systematic synthesis followed by XRD and TEM experimentations of quinary equimolar (CoFeMgMnNi)-oxide, (CoCrFeMnNi)-oxide and its binary, ternary quaternary derivative oxides establish a pattern in terms of evolution of cubic spinel and rocksalt phases, their orientation relationship and microstructural growth during sintering and ageing at different temperatures over varying lengths of time. Quinary multicomponent oxides and its derivatives are metastable in nature, which keep on changing their phase fraction, structural modulation and microstructural growth. A bird eye view of the fundamental nature of these equimolar multicomponent oxides is discussed in the following sections.

5.4.1. Phase evolution and structural correlation between spinel and rock salt

Ternary equimolar mixture of Co(II,III)O, MgO and NiO upon dry milling for 40 h results in a phase mixture of cubic spinel and rocksalt phases. The lattice parameter of the resulting spinel phase is almost double of the rocksalt phase. Initially NiO and MgO oxide act as the host lattice for rocksalt structure, in which CoO is incorporated. In the same line, Co_3O_4 phase with spinel structure acts as the host lattice for the spinel phase in which Ni- and Mg-ions are incorporated. It is further observed that with the progress of milling and solid solution formation, strain induced broadening of diffraction peaks takes place with a concomitant shift in its mean position (Figure 5.1). Shift in the peak position is not uni-directional. Shift in the peak position may directly be associated with the change in d-spacings, lattice parameter and cell volume. It is understood that with the progress of milling, vacancy concentration in the lattice continues to increase. Continuous change in the vacancy concentration in the spinel and in the rocksalt phase is one of the reasons behind the change in the d-spacings, lattice parameter and the cell volume. As the spinel and the rocksalt phases are associated through the vacancy concentration, the relative phase

fraction of spinel and the rocksalt phases changes that leads to a shift in the mean position of the peak. In this connection it is important to explain the structural correlation between the spinel phase and the rocksalt phase. In both the phases, oxygen forms the FCC lattice, in case of the rocksalt phase all the octahedral voids are filled up with cations and in case of the spinel phase half the octahedral voids are filled with cations. This explains that the rocksalt phase may transform to a spinel phase when vacancy concentration is changed and vice versa. After sintering the mixed powder, similar spinel and rocksalt phases are observed in the pellet. On addition of Fe- and Mn-ions in the ternary (CoMgNi)-oxide, i. e. in the quaternary (CoFeMgNi)-oxide and in the (CoMgMnNi)-oxide also similar phase mixture of rocksalt and spinel is observed. However, in quinary (CoFeMgMnNi)-oxide and (CoCrFeMnNi)-oxide predominantly spinel is observed. Predominant spinel phase formation in the quinary oxide may be attributed to the multiple oxidation states of Fe, Cr and Mn and related Jan Teller distortions in the lattice.

5.4.2. Oriented growth of spinel, rocksalt phases and its interface structure

In the (CoMgNi)-oxide after sintering at 1473 K for 10 h, predominantly rocksalt phase with *a~4.2 Å* lattice parameter is observed. In the electron diffraction pattern of the rocksalt phase diffuseness in the primary diffraction spots and minor arcing and split in the higher order spots is observed (Figure 5.4(a-d) and Figure 5.5a). Diffuseness in the primary diffraction spots and split in the higher order spots may be attributed to the residual strain in the rocksalt crystal due to the presence of multiple cations in the phase. Mottled contrast in the BF image (Figure 5.4c) confirms the presence of residual strain the crystal. However, ageing at 723 K for 120 h, results in arcing in the diffraction spots (Figure 5.5b). It may be explained by the formation of structurally modulated domains in the rocksalt phase and a continuous relative rotation between the domains. Structurally modulated domain

formation and relative rotation between them takes place in order to reduce the lattice strain in the crystal. In the corresponding TEM images (Figure 5.4(e-f)) formation of irregular fringe contrast is observed. Inter-fringe spacing may directly be correlated with the stacking of domains with relative in-plane and out-of-plane rotation. Similar domain formation, relative rotation between them has been observed in (CaCoFeMgNi)-oxide and (CoCuMgNiZn)-oxide before.

In quinary (CoFeMgMnNi)-oxide after sintering at 1473 K for 10 h, spinel phase forms predominantly. In the electron diffraction pattern of the spinel phase similar diffuseness in the diffraction spots is observed (Figure 5.7a and Figure 5.7c). When the quinary oxide is sintered for 100 h at 1473 K, modulation of intensity in the diffraction pattern and systematic appearance of extra spots are observed (Figure 5.8a and Figure 5.8e) and it may be directly correlated to the oriented growth of a rocksalt phase within the spinel phase with almost half the lattice parameter of the spinel phase. The interface diagram of the spinel phase with the rocksalt phase has been presented schematically in Figure 5.11. The interface is semi-coherent. It is understood that such orientation relationship develops in a bid to reduce the interface strain through continuous reconstructive transformations at the interfaces. In a similar way, in the (CoCrFeMnNi)-oxide after sintering at 1473 K for 10 h structurally modulated domains (Figure 5.10a-f) are observed with continuous diffuse streaking in the diffraction pattern along 220 type directions. Structural modulations in multicomponent oxides appears to be a common phenomenon which takes place in order to reduce strain in the crystal. The structural and compositional modulations grow with time as has been reported in (CoFeMn)-oxide before [30].

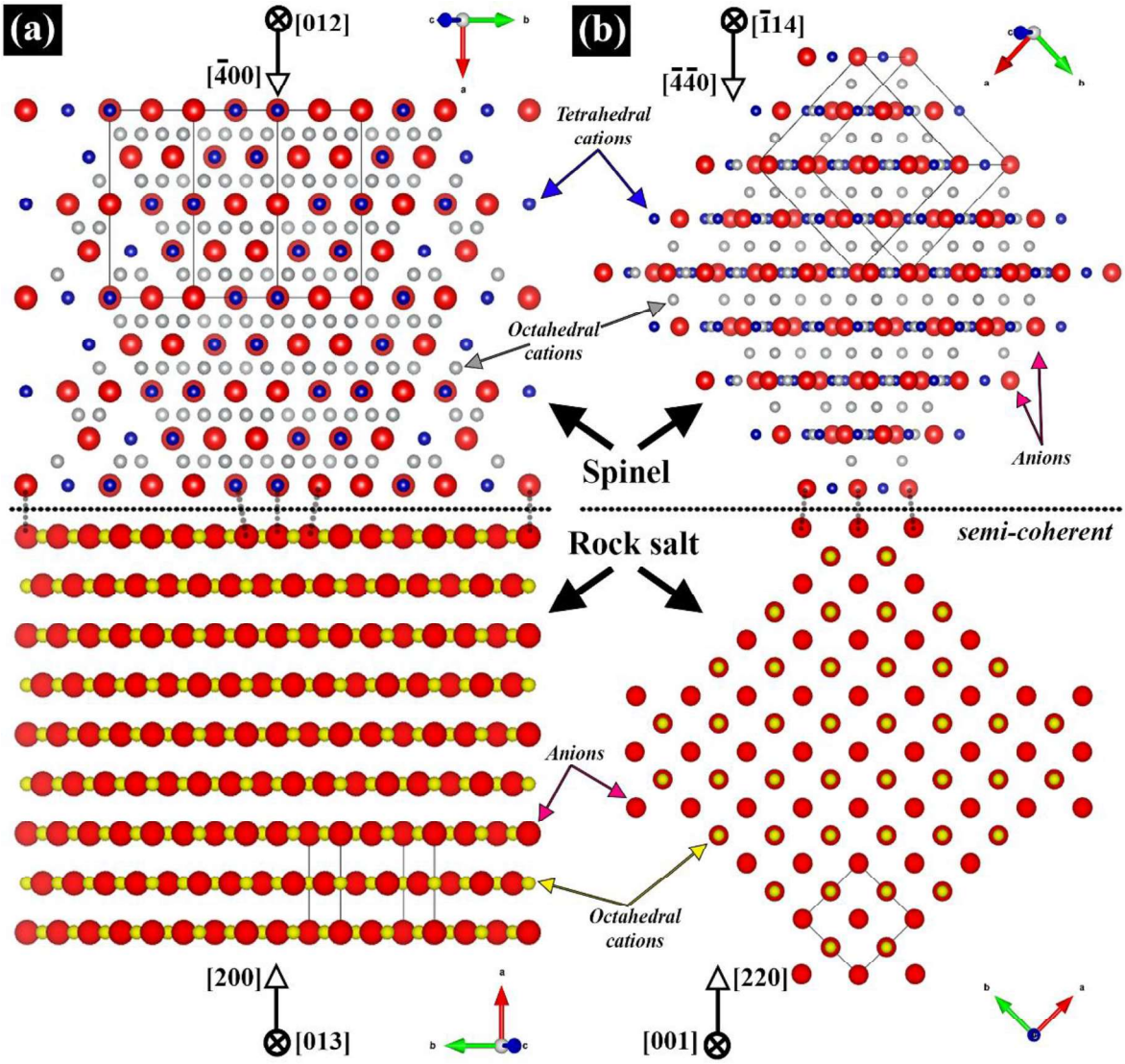

Figure 5.11: Projected interface structure diagram between cubic spinel phase and cubic rocksalt phase. The interface structure diagram has been developed based on the experimentally observed orientation relationship between the cubic spinel phase and the cubic rocksalt phase. The interfaces are semi-coherent in nature.

5.4.3 Stabilization through energy minimization

In the multicomponent quinary (CoFeMgMnNi)-oxide and (CoCrFeMnNi)-oxide, spinel phase forms after sintering. However, with prolonged sintering or ageing oriented growth of rocksalt phase and development of structural modulation is clearly visible. It is also understood that oriented growth and structural modulation takes place in order to minimize strain in the crystal. Quinary multicomponent oxides are metastable and with energy impetus from outside in the form of prolonged exposure at higher temperature, these oxides

try to reduce their energy through minimization of strain in the crystal, which manifests itself as domain formation, their relative rotation, coherent/semi-coherent interface formation etc. Similar trend has been observed for (CaCoFeMgNi)-oxide and (CoCuMgNiZn)-oxide. Multicomponent oxides are believed to be entropy stabilized. However, the authors have noted a complex interplay between entropy and strain energy that leads to the energy minimization. Gibbs free energy may be written as $\Delta G = \Delta H - T\Delta S$, where the symbols have their usual meaning. Further, $\Delta H = \Delta U + P\Delta V$ for a constant pressure process. Combining both the equations, Gibbs free energy equation may be written as $\Delta G = \Delta U + P\Delta V - T\Delta S$. The term $P\Delta V$ represents mechanical energy associated with the transformation. In a multicomponent oxide, due to the presence of several cations in the lattice, configurational entropy is high that maximizes the negative contribution of the $T\Delta S$ term. However, maximizing the entropy comes with a cost of enhanced strain the lattice, which is reflected by the $P\Delta V$ term. In order to make the Gibbs free energy component optimally negative, the system tries to modulate itself compositionally and structurally that reduces the negative contribution of the entropy term. However, through structural and compositional modulations it forms coherent/semi-coherent interfaces and reduces the lattice strain. That is how it reduces the positive contribution of the $P\Delta V$ term. It is a trade-off between the entropy and the strain energy that minimizes the Gibbs free energy of the system. The authors would tend to believe that in multicomponent systems, it is not only the entropy that determines the stability. It is a trade-off between entropy and strain energy that determines the stability of the system.

5.5. Conclusions

High-energy ball-milling sets up a competition between rocksalt and spinel phases which is driven by the build-up of vacancies and its varying concentration in the phases, which keeps on changing with milling time. Equimolar ternary (CoMgNi)-oxide, previously

anticipated as the host structure for the stabilization of quinary phase-pure (CoCuMgNiZn)-oxide with rocksalt structure, co-exists with small volume fraction of spinel phase. Furthermore, it is metastable with respect to intermediate temperature ageing heat treatment, and microstructural features appear due to the formation of intergrown domain structure arising out of successive mutual in-plane and out-of-plane rotations.

Systematic substitution of Mn- and Fe-ions in (CoMgNi)-oxide transforms the global average single-phase with rocksalt structure to a global average single-phase with spinel structure in equimolar (CoFeMgMnNi)-oxide, being reported for the first time. Prolonged exposure to high temperature in (CoFeMgMnNi)-oxide leads to precipitation of a rocksalt phase of half the lattice parameter, which develops according to definite orientation relationships with its parent spinel phase sharing semi-coherent boundaries between them. Structural modulation observed in sintered and quenched equimolar (CoCrFeMnNi)-oxide along <220> crystallographic directions was previously unanticipated. Furthermore, local composition modulation induced formation of nanometer-sized domains, which in turn brings out the shortcomings of the high entropy effect.

5.6. Reference

[1] W. Bian, H. Li, Z. Zhao, H. Dou, X. Cheng, X. Wang, Entropy stabilization effect and oxygen vacancy in spinel high-entropy oxide promoting sodium ion storage, Electrochimica Acta, 2023, 447, 142157 (10 pages)

[2] F. Zhai, X. Zhu, W. Zhang, G. Cao, H. Zhang, Y. Xing, Y. Xiang, S. Zhang, Insight of the evolution of structure and energy storage mechanism of $(FeCoNiCrMn)_3O_4$ spinel high entropy oxide in life-cycle span as lithium-ion battery anode, J. Power Sources, 2024, 603, 234418 (11 pages)

[3] D. Berardan, S. Franger, D. Dragoe, A.K. Meena, N. Dragoe, Colossal dielectric constant in high entropy oxides, Phys. Status Solidi RRL, 2016, 10, 328-333

[4] H. Wu, Q. Lu, Y. Li, J. Wang, Y. Li, R. Jiang, J. Zhang, X. Zheng, X. Han, N. Zhao, J. Li, Y. Deng, W. Hu, Rapid joule-heating synthesis for manufacturing high entropy oxides as efficient electrocatalysts, Nano Lett., 2022, 22, 6492-6500

[5] J. Zhang, J. Yan, S. Calder, Q. Zheng, M.A. McGuire, D.L. Abernathy, R. Ren, S.H. Lapidus, K. Page, H. Zheng, J.W. Freeland, J.D. Budai, R.P. Hermann, Long-range antiferromagnetic order in a rocksalt high entropy oxide, Chem. Mater., 2019, 31, 3705-3711

[6] H. Yang, Q. Chen, J. Zhu, G. Jiang, L. He, N. Qiu, Y. Wang, Selective construction of amorphous/crystalline heterostructure high entropy oxide for Li-ion batteries, J. Alloys Comp., 2024, 986, 174140 (9 pages)

[7] M.P.J. Segura, T. Takayama, D. Berardan, A. Hoser, M. Reehuis,H. Takagi, N. Dragoe, Long-range magnetic ordering in rocksalt-type high-entropy oxides, Appl. Phys. Lett., 2019, 114, 122401-5

[8] C. M. Rost, E. Sachet, T. Borman, A. Moballegh, E.C. Dickey, D. Hou, J.L. Jones, S. Curtarolo, J.P. Maria, Entropy-stabilized oxides, Nat. Commun., 2015, 6, 9485 (8 pages)

[9] J. Dabrowa, M. Stygar, A. Mikula, A. Knapik, K. Mroczka, W. Tejchman, M. Danielewski, M. Martin, Synthesis and microstructure of the $(Co,Cr,Fe,Mn,Ni)_3O_4$ high entropy oxide characterized by spinel structure, Mat. Lett., 2018, 216, 32-36

[10] L. Lin, K. Wang, R. Azmi, J. Wang, A. Sarkar, M. Botros, S. Najib, Y. Cui, D. Stenzel, P.A. Sukkurji, Q. Wang, H. Hahn, S. Schweidler, B. Breitung, Mechanochemical synthesis: route to novel rock-salt-structured high-entropy oxides and oxyfluorides, J. Mater. Sci., 2020, 55, 16879-89

[11] B.L. Musico, D. Gilbert, T.Z. Ward, K. Page, E. George, J. Yan, D. Mandrus, V. Keppens, The emergent field of high entropy oxides: Design, prospects, challenges and opportunities for tailoring material properties, APL Mater., 2020, 8, 040912 (17 pages)

[12] R. J. Clement, Z. Lun, G. Ceder, Cation-disordered rocksalt transition metal oxides and oxyfluorides for high-energy lithium-ion cathodes, Energy Environ. Sci., 2020, 13, 345 (29 pages)

[13] C.M. Rost, D.L. Schmuckler, C. Bumgardner, M.S.B. Hoque, D.R. Diercks, J.T. Gaskins, J.P. Maria, G.L. Brennecka, X. Li, P.E. Hopkins, On the thermal and mechanical properties of $Mg_{0.2}Co_{0.2}Ni_{0.2}Cu_{0.2}Zn_{0.2}O$ across the high-entropy to entropy-stabilized transition, APL Mater., 2022, 10, 121108 (7 pages)

[14] W. Hong, F. Chen, Q. Shen, Y.H. Han, W.G. Fahrenholtz, L. Zhang, Microstructural evolution and mechanical properties of (Mg,Co,Ni,Cu,Zn)O high-entropy ceramics, J. Am. Ceram. Soc., 2019, 102, 2228-2237

[15] J. Lu, K.S. Lee, Spinel cathodes for advanced lithium ion batteries: a review of challenges and recent progress, Mater. Technology, 2016, 1208957 (15 pages)

[16] N.J. Usharani, R. Shringi, H. Sanghavi, S. Subramanian, S.S. Bhattacharya, Role of size, alio-/multi-valency and non-stoichiometry in the synthesis of phase-pure high entropy oxide (Co,Cu,Mg,Ni,Na,Zn)O, Dalton Trans., 2020, 49, 7123 (10 pages)

[17] H. Yang, L. He, Z. Yang, Q. Chen, G. Jiang, J. Zhu, R. Xue, N. Qiu, Y. Wang, Design optimization of spinel-rocksalt intergrown high entropy oxide structure for enhanced electrochemical properties, J. Alloys Comp., 2023, 968, 172135 (12 pages)

[18] A.D. Dupuy, M.R. Chellali, H. Hahn, J.M. Schoenung, Nucleation and growth behaviour of multicomponent secondary phases in entropy-stabilized oxides, J. Mater. Res., 2023, 38, 198-214

[19] A.D. Dupuy, I.T. Chiu, P. Shafer, E. Arenholz, Y. Takamura, J.M. Schoenung, Hidden transformations in entropy-stabilized oxides, J. Eu. Ceram. Soc., 2021, 41, 6660-6669

[20] Z. Rak, J.P. Maria, D.W. Brenner, Evidence for Jahn-Teller compression in the (Mg,Co,Ni,Cu,Zn)O entropy-stabilized oxide: A DFT study, Mat. Lett., 2018, 217, 300-303

[21] M. Frachhia, M. Coduri, M. Manzoli, P. Ghigna, U.A. Tamburini, Is configurational entropy the main stabilizing term in rock-salt $Mg_{0.2}Co_{0.2}Ni_{0.2}Cu_{0.2}Zn_{0.2}$ high entropy oxide, Nat. Commun., 2022, 13, 2977 (4 pages)

[22] G. Anand, A.P. Wynn, C.M. Handley, C.L. Freeman, Phase stability and distortion in high-entropy oxides, Acta Mater., 2018, 146, 119-125

[23] Z. Grzesik, G. Smola, M. Stygar, J. Dabrowa, M. Zajusz, K. Mroczka, M. Danielewski, Defect structure and transport properties in (Co,Cu,Mg,Ni,Zn)O high entropy oxide, J. Eu. Ceram. Soc., 2019, 39, 4292-4298

[24] J. Baek, M.D. Hossain, P. Mukherjee, J. Lee, K.T. Winther, J. Leem, Y. Jiang, W.C. Chueh, M. Bajdich, X. Zheng, Synergistic effects of mixing and strain in high entropy spinel oxides for oxygen evolution reaction, Nat. Commun., 2023, 14, 5936 (11 pages)

[25] A. Navrotsky, O.J. Kleppa, The thermodynamics of cation distributions in simple spinels, J. Inorg. Nucl. Chem., 1967, 29, 2701-2714

[26] Y. Horibe, S. Takeyama, S. Mori, Large-scale phase separation with nano-twin domains in magnetite spinel $(Co,Fe,Mn)_3O_4$, AIP conf. Proc., 2016, 1763, 050005 (5 pages)

[27] P.K. Davies, M. Akaogi, Phase intergrowths in spinelloids, Nature, 1983, 305, 788-790

[28] K. E. Sickafus, J.M. Wills, N.W. Grimes, Spinel compounds: Structure and property relations, J. Am. Ceram. Soc., 1999, 82, 3279-92

[29] A. Singh, S. Yasui, A.S. Pal, L.A. Bendersky, I. Takeuchi, R.K. Mandal, J. Basu, Structure and interfaces of compositionally graded $Li(Ni,Mn)_xO_y$ cathodes on (111) Nb-doped $SrTiO_3$, Philosophical Magazine, 2022, 102, 1547-1579

[30] A.S. Pal, A.K.L. Das, K. Gururaj, M. Sadhasivam, K.M. Knowles, Md. I. Ahmad, K.G. Pradeep, J. Basu, Nanoarchitectonics of self-assembled chessboard-like structures by recurrent phase separation and coalescence of nano domains in CoFeMn oxide, Acta Mater., 2023, 242, 118423 (12 pages)

[31] D. Berardan, A. K. Meena, S. Franger, C. Herrero, N. Dragoe, Controlled Jahn-Teller distortion in (MgCoNiCuZn)O-based high entropy oxides, J. Alloys Comp., 2017, 704, 693-700

[32] S. Mukherjee, N.K. Mukhopadhyay, J. Basu, Local composition modulation and oriented inter-growth induced strain minimization in entropy stabilized (CoCuMgNiZn) oxide [Communicated]

[33] S. Mukherjee, N.K. Mukhopadhyay, J. Basu, Composition modulation, strain minimization and oriented growth of phases in equimolar (CaCoFeMgNi) multicomponent oxide, Acta Mater., 2025, 285, 120621 (12 pages)

[34] B. Cantor, I. T. H. Chang, P. Knight, A. J. B. Vincent, Microstructural development in equiatomic multicomponent alloys, Mater. Sci. Eng. A, 2004, 375-377, 213-218

[35] A. S. Pal, A. K. L. Das, A. Singh, K. M. Knowles, M. I. Ahmad, J. Basu, Evolution of a self-assembled chessboard nanostructure spinel in a CoFeGaMnZn multicomponent oxide, Philos. Mag., 2022, 102(12), 1121-1135